

EXTINCTION AND DISTANCE TO ANOMALOUS X-RAY PULSARS FROM X-RAY SCATTERING HALOS

A. RIVERA-INGRAHAM AND M. H. VAN KERKWIJK

Department of Astronomy & Astrophysics, University of Toronto, 50 Saint George Street, Toronto, ON M5S 3H4, Canada
Draft version September 16, 2018

ABSTRACT

We analyze the X-ray scattering halos around three Galactic Anomalous X-ray Pulsars (AXPs) in order to constrain the distance and the optical extinction of each source. We obtain surface brightness distributions from EPIC-pn data obtained with *XMM-Newton*, compare the profiles of different sources, and fit them with a model based on the standard theory of X-ray scattering by dust grains, both for a uniform distribution of dust along the line of sight, and for dust distributions constrained by previous measurements. Somewhat surprisingly, we find that for all three sources, the uniform distribution reproduces the observed surface brightness as well as or better than the distributions that are informed by previous constraints. Nevertheless, the inferred total dust columns are robust, and serve to confirm that previous measurements based on interstellar edges in high-resolution X-ray spectra and on modelling of broad-band X-ray spectra were reliable. Specifically, we find $A_V \simeq 4, 6$, and 8 mag for 4U 0142+61, 1E 1048.1–5937, and 1RXS J170849.0–400910, respectively. For 1E 1048.1–5937, this is well in excess of the extinction expected towards a H I bubble along the line of sight, thus casting further doubt on the suggested association with the source.

Subject headings: stars: individual (4U 0142+61, 1E 1048.1–5937, 1RXS J170849.0–400910) – stars: neutron – dust, extinction – scattering

1. INTRODUCTION

Among the diversity of objects comprising the neutron star family, Anomalous X-ray Pulsars (AXPs) are one of the two classes of magnetars, with their emission powered by the decay of extremely strong magnetic fields, of 10^{14} – 10^{16} G, whose origin is still a matter of debate (for a review, Woods & Thompson 2006). As remnants of massive, short-lived stars, these sources lie preferentially near the Galactic Plane and thus are strongly absorbed, hindering measurements of their intrinsic spectra and luminosities. In some cases, distances and extinction columns could be estimated from associated supernova remnants (1E 2259+586, Gregory & Fahlman 1980; Kothes, Uyaniker, & Yar 2002; 1E 1841–045, Vasisht & Gotthelf 1997) and other structures (1E 1048.1–5937, Gaensler et al. 2005).

More recently, Durant & van Kerkwijk (2006a,b, hereafter DvK06a,b) tried to determine the extinctions and distances to the sources more directly, by measuring the extinction from absorption edges in high-resolution X-ray spectra, and inferring distances by comparison with the run of extinction with distance as inferred from red clump stars near the line of sight. They found that all AXPs were located in spiral arms (not surprising given their youth) and that their luminosities were remarkably uniform, near 10^{35} erg s^{−1}. Comparing the inferred distances to earlier work, the results were consistent for 1E 1841–045 and XTE J1810–197 (for the latter a distance from H I absorption was available), but inconsistent for 1E 2259+586 and 1E 1048.1–5937. For 1E 2259+586, DvK06a argued that the associated supernova remnant CTB 109 could be at the larger distance of ~ 7.5 kpc instead of the ~ 3 kpc inferred by Kothes et al. (2002), while for 1E 1048.1–45937, they concluded that,

at ~ 9 kpc, the source was not associated with the H I bubble at ~ 2.7 kpc found by Gaensler et al. (2005), even though it appeared fairly nicely centered on it.

Of course, it is possible that the analysis of DvK06a,b was flawed. The underlying assumptions are that the extinction measures are reliable, that they reflect only interstellar extinction, and that the run of interstellar extinction with distance can be reliably inferred from red clump stars. The latter assumption is perhaps the safest, since the red clump stars are fairly well-understood standard candles. The extinction measures are relatively uncertain, however, especially for 1E 1048.1–5937, which relied on fitting of the broad-band X-ray spectrum and is thus sensitive to the assumed intrinsic model (see DvK06b). Furthermore, if a large part of the extinction were local to the source, and thus not present along the lines of sight to the red clump stars, the distances would be overestimated.

Here, we seek to test the extinctions and distances using X-ray scattering halos, which appear as diffuse emission around an X-ray point source and arise from small-angle scattering of soft X-rays by dust in the line of sight (Overbeck 1965). X-ray halo analyses have been carried out on a variety of galactic and extragalactic objects (Mauche & Gorenstein 1986; Predehl & Schmitt 1995), and have proven to be particularly useful in constraining the properties of dust grains in the ISM. For variable sources, where the time delays in the scattering halo could be measured, they have also been used to determine distances (Predehl et al. 2000, Xiang, Lee, & Nowak 2007).

For our purposes, the benefit of the scattering halo is mostly that it provides a column density that is purely interstellar, since we can only measure the halo outside the point-spread function (at $\gtrsim 0.5$ for our *XMM-Newton* data), well beyond where dust associated with the source

would contribute. Below, we will find that the intensities of the halos confirm the extinction estimates of DvK06b, and that, therefore, there is little extinction local to the source. In principle, it should also be possible to use the detailed structure of the halo to check the run of extinction with distance inferred from the red-clump stars. Here, however, we find that, generally, the X-ray halos are fit just as well, or even better, with dust distributions more uniform than indicated by the data, perhaps because simplifications made in our modelling of the dust removed some of the variety that would have smoothed the structure further.

The layout of this paper is as follows. In § 2, we first describe the model we use for fitting the X-ray observations. Next, in § 3, we describe how we measured the radial surface brightness profiles from archival *XMM-Newton* data and, in § 4, how we fit these with our model, discussing some consistency checks and possible pitfalls. We conclude in § 5.

2. EXPECTED SURFACE BRIGHTNESS DISTRIBUTIONS

We model the observed surface brightness distributions for each source with three components, an unscattered central point source, a halo of light scattered by dust, and unrelated background emission. Below, we discuss our assumptions for the halo in more detail; for the point source, we will use measurements of an unabsorbed source, and for the background, we will assume it is independent of position.

The scattering of X rays on dust particles is, generally, a complicated problem, and below we follow previous work in making a number of simplifications, most of which are reasonable as long as one considers X rays with energies above ~ 1 keV. For our sources, this also implies the single-scattering limit is appropriate.

Assuming that the dust grains are spherical, one can write the scattered intensity observed at an angular distance θ_{obs} from the central source as (Smith & Dwek 1998),

$$I(\theta_{\text{obs}}) = F_X \int_{E_{\text{min}}}^{E_{\text{max}}} S(E) dE \int_{a_{\text{min}}}^{a_{\text{max}}} N_H n(a) da \times \int_0^1 \frac{\tilde{f}(x)}{(1-x)^2} \frac{d\sigma(E, a, \theta_{\text{scat}})}{d\Omega} dx, \quad (1)$$

where F_X and $S(E)$ are the observed flux and normalised spectrum in the energy range $[E_{\text{min}}, E_{\text{max}}]$; a is the grain radius and $n(a)$ the corresponding number density; x is the distance from the observer normalised by the distance to the source (see, e.g., Fig. 1 in Mathis & Lee 1991); $\tilde{f}(x)$ is the normalized spatial distribution of the scattering sites (equal to 1 if evenly distributed); and $d\sigma(E, a, \theta_{\text{scat}})/d\Omega$ is the differential scattering cross section, with θ_{scat} the angle over which the X ray is scattered. For small angles, $\theta_{\text{scat}} = \theta_{\text{obs}}/(1-x)$; hence, generally, the innermost regions of the halo are due to dust grains close to the source, while the outer regions are due to grains closer to the observer.

In the above integral, the least-known parts are the dust size distribution and the scattering cross section, both of which depend on the physical state and composition of the dust grains. For the former, following Mathis, Rumpl, & Nordsieck (1977), generally a power-

law form is assumed, while for the latter either the Gaussian approximation of the Rayleigh-Gans theory is used (hereafter RG; e.g., Overbeck 1965), or a more detailed calculation is done using Mie theory (van de Hulst 1957). In the RG approximation, it is assumed that reflection from the grain surface is negligible and that the phase of the incident wave is not shifted inside the medium, resulting in coherent addition of the scattered waves. Smith & Dwek (1998) have shown that for $E \gtrsim 1$ keV and small scattering angles, the approximation agrees well with Mie theory, while for lower energies, RG theory underpredicts the scattering efficiency.

In our work, we will assume the RG approximation, and limit ourselves to relatively high energies. Specifically, we approximate the cross section by (van de Hulst 1957),

$$\frac{d\sigma(E, a, \theta_{\text{scat}})}{d\Omega} \simeq C_{\text{dust}} a^6 \exp\left(-\frac{\theta_{\text{scat}}^2}{2\tilde{\sigma}^2}\right), \quad (2)$$

where the constant of proportionality C_{dust} depends on dust parameters such as the atomic charge, mass number, density, and scattering factor (e.g., Henke et al. 1982), and $\tilde{\sigma}$ indicates the typical size of the halo produced by grains with radius a , given by (Mauche & Gorenstein 1986),

$$\tilde{\sigma} = 10.4 \text{ arcmin} \frac{1}{(E/1 \text{ keV})(a/0.1 \mu\text{m})}. \quad (3)$$

As an aside, we note that with this cross-section, and for $\tilde{f}(x) = 1$, the integral over x in Eq. 1 can be expressed in terms of the error function. Furthermore, the integral over annuli required to obtain mean surface brightnesses around some θ_{obs} , can also be expressed easily. Specifically,

$$\int_{\theta} \theta d\theta \int_x \frac{1}{(1-x)^2} \exp\left(-\frac{1}{2} \left(\frac{\theta}{\tilde{\sigma}(1-x)}\right)^2\right) dx = \tilde{\sigma} \theta \frac{\text{erf}(\tilde{\alpha})}{\sqrt{2/\pi}} + \tilde{\sigma}^2 (1-x) \exp(-\tilde{\alpha}^2), \quad (4)$$

where we defined $\tilde{\alpha} = \theta/\sqrt{2}\tilde{\sigma}(1-x)$. With this expression, to calculate the expected halo brightnesses for piece-wise uniform dust distributions $\tilde{f}(x)$, we only need to integrate numerically over a and E .¹

For the dust size distribution, we use a power law $n(a) \propto a^q$ with two different choices for the power and lower and upper limits. For our primary model, we set $q = -3.5$, following the finding of Mathis et al. (1977), and use $a_{\text{min}} = 0.005 \mu\text{m}$ and $a_{\text{max}} = 0.25 \mu\text{m}$ (informed by the work of, e.g., Costantini et al. 2005). This model yields a halo dominated by somewhat larger grains than found in the fits of Predehl & Schmitt (1995), whose calibration of scattering optical depth with optical extinction we will use. Therefore, to see how strongly our results depend on our choice, we also try a somewhat steeper power, $q = -4$, and smaller maximum grain size, $a_{\text{max}} = 0.18 \mu\text{m}$, more similar to the values typically found by Predehl & Schmitt. Finally, we fit profiles in

¹ For power-law dust distributions $n(a) \propto a^q$ with integral power q , the integral over a can also be expressed in terms of error functions.

TABLE 1
XMM-NEWTON IMAGING DATA USED

Source	Obs. ID	Filter	Exp. (ks)	b^{II} ($^{\circ}$)	A_V (mag)	d (kpc)
<i>Anomalous X-ray Pulsars</i>						
4U 0142+61	0112781101	Thin	4.2	-0.43	3.5 ± 0.4	3.6 ± 0.4
1E 1048.1-5937	0510010601	Thin	32	-0.52	5.6 :	9.0 ± 1.7
1RXS J170849.0-400910	0148690101	Medium	30	+0.03	7.7 ± 2.2	3.8 ± 0.5
<i>Empirical PSF</i>						
PKS 2155-304	0080940301	Thin	39	-52.25
	0158961301	Medium	39	-52.25

NOTE. — All observations used EPIC-pn in the small window mode. The exposure time is the total time not affected by flaring. For reference, the galactic latitude b^{II} is listed, as well as the extinction A_V and distance d inferred by Durant & van Kerkwijk (2006a,b). No error is listed for the extinction for 1E 1048.1-5937, since it is based on a fit to broad-band X-ray data and the uncertainty is thus dominated by the extent to which the assumed intrinsic emission model is correct.

narrow energy ranges, so that we can ignore the dependence on the spectral shape $S(E)$ in our integration over energy.

For given $\tilde{f}(x)$, the above suffices to describe the radial profile of the halo, and our fits yield the normalisation. Integrating the shape over θ_{obs} then yields the total observed intensity of the halo, I_{halo} , which is related to the scattering optical depth τ_{scat} by,

$$\frac{I_{\text{halo}}}{I_{\text{halo}} + I_{\text{core}}} = 1 - \exp(-\tau_{\text{scat}}), \quad (5)$$

where I_{core} is the unscattered intensity of the point source.

We normalize the scattering optical depth to 1 keV using that $\tau_{\text{scat}} \propto E^{-2}$, and convert to equivalent visual extinction using the empirical calibration² derived from 29 Galactic sources by Predehl & Schmitt (1995),

$$\tau_{\text{scat}, 1 \text{ keV}} = A_V(0.079 \pm 0.003) - (0.052 \pm 0.019). \quad (6)$$

We note that no offset would be expected, and its presence may reflect the use of the RG approximation even at energies below 1 keV, where it is known to be inaccurate (P. Predehl, 2008, pers. comm.). The resulting systematic uncertainties are compensated to some extent, however, by the fact that the assumptions we make are very similar to those of Predehl & Schmitt (1995), causing us to make errors in the same direction. Furthermore, assuming that the dust properties do not vary wildly between different lines of sight, the same should hold between our different sources, i.e., the relative intensities of the halos should provide a good measure of the relative dust columns.

3. OBSERVED SURFACE BRIGHTNESS DISTRIBUTIONS

In order to measure the scattering halos, we need good angular resolution and sensitivity, yet avoid non-linearity in the bright, unscattered light. These constraints are best met by data taken with the European Photon Imaging Camera with PN detectors (EPIC-PN; Strüder et al. 2001) onboard *XMM-Newton* (*XMM*). Most AXPs – and most good reference sources – are bright and thus observed with small-window mode to avoid pile-up. This

helps to define the surface brightness accurately close to the source, but also implies we cannot measure the halo’s full extent. In the *XMM* archive, suitable observations are available for five of the six well-studied anomalous X-ray pulsars,³ but two of those (1E 1841-045 and 1E 2259+586) are associated with supernova remnants, the emission of which makes it very difficult to measure the scattering halo. Hence, we limited ourselves to the three remaining sources, 1E 1048.1-5937, 4U 0142+61 and 1RXS J170849.0-400910; see Table 1. As a reference source to define the point-spread function, we used the BL Lac PKS 2155-304, which is at high galactic latitude and thus has a negligibly small scattering halo, and which has been observed regularly in different filters.

For all sources, we reprocessed the raw data with the standard pipelines `epchain` and `emchain` from `xmmsas` version 7.1.0 (and the calibration files available with that release). We obtained the surface brightness distributions by summing counts in concentric annular regions of $10''$ width around the source, with the innermost annulus starting at $6''.62$ (avoiding the central parts, where systematic differences due to small centering errors or pile-up effects (see below) are expected to dominate) and the outermost ending at $196''.62$. We selected events within given energy ranges using standard constraints for EPIC-PN (singles and doubles, and no warning flags). We corrected for out-of-time (OoT) events by subtracting an appropriately scaled radial profile, produced from simulated out-of-time only event lists (made with `epchain`; we used the scale factor of 0.011 listed in the *XMM-Newton* Users Handbook for small-window mode). We converted to surface brightnesses by dividing by the areas, using the `arfgen` and `backscale` tasks to ensure the areas include only the parts of the annuli that overlap the detector.

A possible issue with our method, pointed out by the referee, is that the correction for out-of-time events might be unreliable if the source suffers from pile-up. This is because our analysis relies on the fact that photons detected “out of time” – during the transfer from the

² The relation given here supercedes the different numbers given in the text and abstract of Predehl & Schmitt (1995); P. Predehl, 2008, pers. comm.

³ The sixth, XTE J1810-197, has only large-window data, for which there are no corresponding data of our point-spread function reference. We tried to analyze it using the PSF derived from small-window data, but could not find a good model for the scattering halo. This might be because of the different modes, the source’s variability, or a break-down in our model. We did not investigate this further.

imaging part of the CCD to the storage area – have the same rate and spectrum as those measured during the integration. If pile-up occurs, however, the measured source event rate is reduced and the measured spectrum hardened, and thus one would underestimate the rate of low-energy, out-of-time events. Fortunately, for our observations, all taken in small-window mode, pile-up is not an issue (for our brightest source, 4U 0142+61, the total count rate is $\sim 50 \text{ s}^{-1}$, while in small window mode, with its read-out rate of 175 frames per second, pile-up becomes significant only for rates in excess of $\sim 100 \text{ s}^{-1}$; we confirmed pile-up is not an issue using the `epatplot` task). Nevertheless, it would be a problem for brighter sources and/or imaging modes with longer integration times. In those cases, it would likely be best to measure the radial profile in areas excluding all parts affected by out-of-time events (i.e., excluding a strip along the read-out direction that passes over the source).

4. SCATTERING HALOS

To derive halo intensities, we fit our radial profiles with a combination of an empirical PSF, the scattering halo model for a variety of assumed distributions of dust along the line of sight (and for two dust size distributions; see §2), and a constant background. We fit the radial profile in two energy ranges simultaneously, 1.2–1.6 and 2.0–2.4 keV. Here, the lower range will have the stronger dust scattering signal (yet is at sufficiently high energy that multiple scattering is not a significant issue for the sources considered here), but, given the small field of view, it is mostly sensitive to dust close to the source. The higher energy range will have a weaker scattering halo (though still noticeable), but helps to constrain the dust somewhat closer to the observer, as well as to verify consistency.

We used the radial profiles from the observations of the high latitude source PKS 2155–304 as the empirical PSF in the fitting routines. The main advantages over using a theoretical PSF are that one automatically minimizes any common artefacts (either instrumental or due to the analysis method; see, e.g., the wiggles at large radial distances in the right-hand panels of Figs 2, 4, and 6), artefacts not necessarily captured in a theoretical PSF model. A disadvantage is that, effectively, the fits now measure relative brightnesses and background levels. In order to put these on an absolute scale, we determined the backgrounds and normalizations for our calibrator by fitting its profiles using the theoretical PSF of Ghizzardi (2002, a King profile with energy and position-dependent width and exponent).

For the dust distributions along the line of sight, we try two types. First, we use a uniform distribution, in which the halo contribution depends only on the total amount of dust. Second, we try a variety of piece-wise uniform distributions, constrained to follow the run of reddening with distance inferred from red clump stars by DvK06a. Here, the halo intensity depends on distance, which determines both the total dust column, and the fractional distances of the boundaries between the different pieces. Since the halo is fairly sensitive to the precise spatial distribution of dust, we chose up to three different distributions. For the first – model A – we always tried to match the DvK06a results exactly (to the extent possible without having unphysical decreases of dust column with

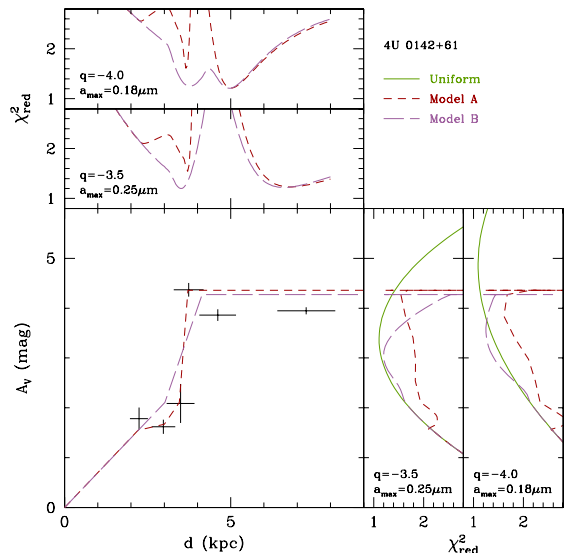


FIG. 1.— Extinction and distance for 4U 0142+61. In the main panel, the run of extinction with distance is shown, as inferred from red-clump stars by DvK06a. Overdrawn are two piece-wise uniform approximations we used to fit the halo intensity (models A and B). In the top panels, we show for both models how the reduced χ^2 of the fit to the observed radial profiles varies with distance, for two choices of dust distribution (as indicated). In all cases, two minima appear, between 4 and 6 kpc. In the right-hand panels, we show the implied variations in χ^2_{red} with total extinction for both models and both dust distributions, as well as the results for a uniform dust distribution (for which the predicted scattering halos does not depend on distance). For all models, one infers $A_V \simeq 4 \text{ mag}$.

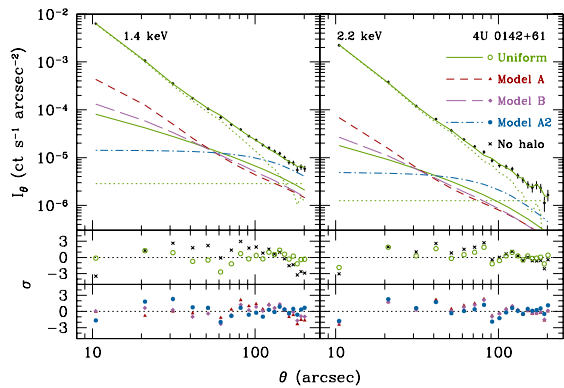


FIG. 2.— Radial profiles of 4U 0142+61 in the 1.2–1.6 keV (left) and 2.0–2.4 keV (right) ranges, fitted with a combination of an empirical PSF, a scattering halo for a variety of models, and a constant background. The green lines reflect the fit for a uniform distribution, with the dotted lines showing the unscattered and background components, and the solid lines the contribution from the halo and the total of all contributions. The best-fit halo contributions from other models are also shown (as labelled). In the two lower panels, deviations from the various fits are shown, with the residuals for fits using no halo or a halo for uniform dust in the middle panel, and those for fits for piece-wise linear dust distributions in the lowest panel. Note that model A2 refers to the second minimum at large distance found for model A (see Fig. 1).

distance). Since we found that sharp changes provided worse fits, we also tried up to two further models – B and C – both chosen to be “softer,” yet still consistent with the measurements of DvK06a. Combined, these models give a good sense of the sensitivity of our results to such

choices.

In total, any individual fit has five free parameters: two unscattered source intensities and two background brightnesses (one for each of the two energy ranges), and either the total dust column or distance (which determines the fractional halo intensities). In practice, in our fits for uniform density, the five parameters are determined simultaneously by linear least-squares, while for those with varying dust distributions, we step through distance, and for each distance calculate the expected fractional halo contribution and fit for the corresponding best-fit unscattered source intensities and backgrounds.

We show our fit results in Figs. 1–6, and summarize numerical results for our primary dust distribution (with $q = -3.5$ and $a_{\max} = 0.25 \mu\text{m}$) in Table 2. Two conclusions stand out: (i) fits without a halo are much poorer than those with a halo; and (ii) the fractional intensity of the halo increases as expected from the reddening inferred from the X-ray spectra, with 4U 0142+61 having the smallest halo signal, 1E 1048.1–5937 an intermediate one, and 1RXS J170849.0–400910 the largest. Below, we describe the results for the individual sources in detail, and then discuss possible model caveats and systematic uncertainties.

4.1. 4U 0142+61

One of the brightest and most studied AXPs is 4U 0142+61. Absorption edges in its high-resolution X-ray spectrum indicate a total extinction $A_V = 3.5 \pm 0.4$ (DvK06b), which, combined with the run of extinction with distance inferred from the red clump stars, suggests a distance of about 3.5 kpc, in a region of rapidly increasing optical extinction, presumably a spiral arm (DvK06a; see Fig. 1). Thus, we expect that a large fraction of the dust along the line of sight is close to the source, which should affect the inner parts of the halo in particular.

In Fig. 1, we show how χ^2 varies as a function of reddening and distance. For uniformly distributed dust with our primary dust size distribution ($q = -3.5$ and $a_{\max} = 0.25 \mu\text{m}$), there is a clear minimum around $A_V \simeq 4.2$ mag, close to the value inferred spectroscopically. The piecewise uniform models also show consistent minima, with reddening of 3–4 mag and distances of ~ 3.6 kpc. However, they also have secondary minima at larger distances, of ~ 6.7 kpc. Given that AXPs are young and thus likely to reside in spiral arms, the first minimum almost certainly is the correct one.

For our second dust size distribution ($q = -4$ and $a_{\max} = 0.18 \mu\text{m}$), we find fits of similar quality, but somewhat larger values of the extinction. This is as expected: for smaller grains, more of the halo will be outside our field of view, and hence a stronger halo is required to match the observed halo contribution inside the field of view. From these, we conclude the uncertainty due to the dust distribution is considerable, although the results do not change qualitatively.

In Fig. 2, we show the fits to the radial profile, as well as the residuals. From the different halo curves, one sees how larger quantities of dust concentrated towards the source increase the innermost parts of the halo compared to the outer wings. Indeed, both piecewise models give very poor fits if the source is placed near the far end or just behind the rapid rise of extinction around 3.7 kpc inferred from the red clump stars. For the best fits, how-

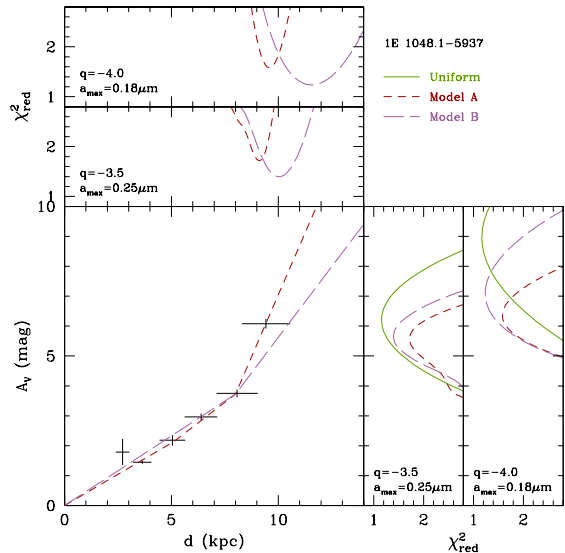


FIG. 3.— Like Fig. 1, but for 1E 1048.1–5937. Note that both approximations to the run of reddening with distance use linear extrapolation beyond $A_V \simeq 6$ mag. The fits indicate a total extinction of about 6 mag for our primary dust size distribution, and a distance of ~ 10 kpc.

ever, the residuals are rather similar, since the changes in halo shape can be compensated to some extent by changes in the other parameters, in particular the background. Note that in the higher energy range, the halo is already very weak compared to the source: its fractional intensity is about 5%.

One surprise is that the uniform model gives a better fit than the two piecewise uniform ones, even though the latter presumably are closer to reality (as inferred from the red-clump stars). Below, we find that smoother distributions also fit better for the other sources. We briefly return to this in §5, but stress here again that among all models, the total extinction is fairly similar.

4.2. 1E 1048.1–5937

One of the main goals of the present study was to test the extinction and distance estimates for 1E 1048.1–5937. Based on the coincidence with a H I bubble, Gaensler et al. suggested a distance of ~ 2.7 kpc, but the high extinction measured for this source, $A_V \simeq 6$, combined with the run of extinction with distance, suggests a much larger distance of ~ 9 kpc (DvK06a).

A major uncertainty is the estimate of the extinction, since it was based on broad-band X-ray fits, and thus necessarily dependent on the assumed underlying source model. Unfortunately, the source was not bright enough to detect absorption edges in its grating X-ray spectra (DvK06b). Visual inspection of observed radial profile of 1E 1048.1–5937, however, already suggests the extinction is indeed fairly high: the source clearly has a contribution due to a scattering halo at least as large as 4U 0142+61 (compare, e.g., the offset around $60''$ from the point-spread function in Figs 2 and 4).

This is confirmed by our scattering halo fits (Fig. 3): all require A_V around 6 mag (somewhat higher for our secondary choice of dust distribution; note, though, that for those we had to extrapolate the run of extinction with distance beyond the range covered by the red clump

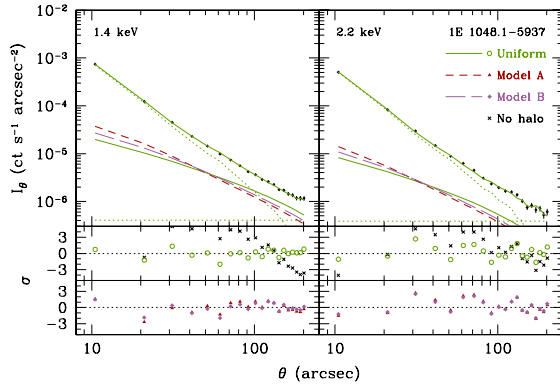


FIG. 4.— Like Fig. 2, but for 1E 1048.1–5937.

stars). Thus, like for 4U 0142+61, we find that the scattering halos are consistent with the total extinction inferred from the X-ray spectrum, and, based on the red-clump stars, the inferred distance remains high, ~ 10 kpc.

The high extinction (and strong halo) are inconsistent with the extinction found from the red-clump stars at 2.7 kpc. The explanation can also not be that there is strong extinction close to the source, since this dust would contribute only to the very inner parts of the halo, and thus not to the halo measured in our fit.

Comparing the different halo models in detail, we find again that the fit for the more uniform dust distributions is the best. Indeed, following precisely the run of extinction with distance inferred by DvK06a, the fit is rather poor, with reduced $\chi^2 \simeq 1.7$. From the halos and residuals in Fig. 4, one again sees that the sharper increase in A_V near the source leads to a halo that is less consistent with the observed one at small angles.

4.3. 1RXS J170849.0–400910

Along the line of sight to 1RXS J170849.0–400910, DvK06a inferred large jumps in reddening from the red clump stars (Fig. 5), likely associated with the Carina and Crux spiral arms. Given $A_V = 7.7 \pm 2.2$ inferred from absorption edges in the X-ray spectrum (DvK06b), the source should be inside the Crux spiral arm, at 3.8 ± 0.5 kpc.

Our fits generally reproduce the above, with A_V between 8 and 9 mag, and the distance around 4 kpc. Again, however, the fits are much better for smoother dust distributions (Fig. 5, Table 2). Indeed, if we assume the exact dust distribution inferred from the red clump stars, we obtain an unacceptable fit, with reduced $\chi^2 \simeq 2.6$. In Fig. 6, one sees that the poor fit is due to the sharp increase in reddening near the source, which causes a halo that is too strong and too flat at small angles compared to what is required by the observations.

4.4. Background Consistency Check

Within the small, $\sim 256 \times 260$ arcsec area covered by our small-window mode observations, the profiles barely reach the background, even without a scattering halo. With a halo, which has a typical size $2\tilde{\sigma} \simeq 1000''$ at 1.4 keV, the profile extends well outside. Thus, one cannot determine the background from an “empty” region, which is why we left it as a free parameter.

Nevertheless, some consistency checks are possible.

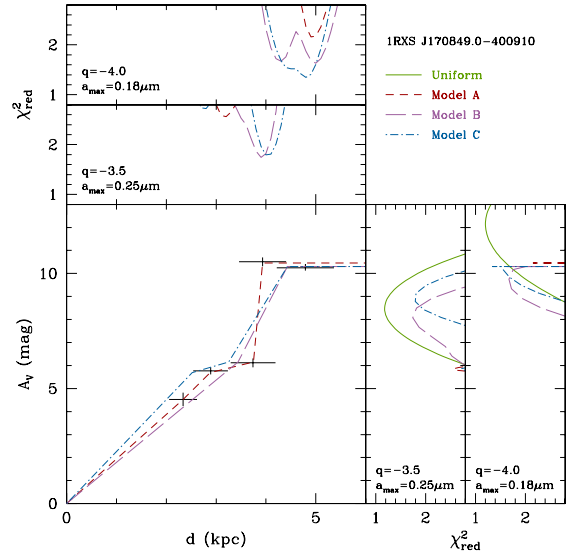


FIG. 5.— Like Fig. 1, but for 1RXS J170849.0–400910. Here, three piece-wise uniform approximations are shown. For model A, most fits have χ^2_{red} values outside of the range shown in the top and right-hand panels. From the other models for our primary dust size distribution, one infers $A_V \simeq 8$ mag and $d \simeq 4$ kpc.

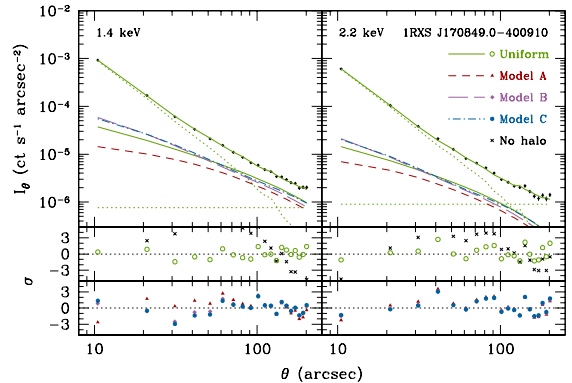


FIG. 6.— Like Fig. 2, but for 1RXS J170849.0–400910.

Easiest perhaps would be to compare with background estimates found in the outer regions of EPIC-MOS exposures taken simultaneously with the PN observations. Unfortunately, we found that those ratios were not constant, probably at least in part due to detector and position dependent instrumental backgrounds (Carter & Read 2007). A rough sense can be obtained from blank fields, even though no templates are available for small-window mode. These show that the typical backgrounds in the two energy bands considered are both $\sim 0.5 \times 10^{-6} \text{ s}^{-1} \text{ arcsec}^{-2}$, with at least a factor 2 variation between different observations.⁴ These are roughly consistent with the rates we infer from our fits (see Table 2).

A stronger constraint might be set by comparing the rates between different energy bands. This is because, as found by Katayama et al. (2004), the spectrum of the background has no strong dependence on intensity, at least at $\gtrsim 1.7$ keV. Indeed, for our calibrator, we find that

⁴ http://xmm2.esac.esa.int/external/xmm_sw_cal/background/index.shtml

TABLE 2
X-RAY SCATTERING HALO FITS

Model ^a	$f_{1.4}$ (s ⁻¹)	$f_{2.2}$ (s ⁻¹)	$b_{1.4}$ (10 ⁻⁶)	$b_{2.2}$ (10 ⁻⁶)	A_V (mag)	d (kpc)	χ^2_{red} ^b
<i>4U 0142+61</i>							
No halo	13.06	4.68	7.0	1.9	3.4
Uniform	12.59	4.58	2.9	1.3	3.4	...	1.1
A	11.87	4.51	4.7	1.5	4.2	3.7	1.5
A2	12.87	4.60	0.1	0.7	4.4	6.8	1.2
B	12.47	4.57	4.0	1.4	3.0	3.5	1.2
B2	12.87	4.60	0.3	0.8	4.3	6.6	1.2
<i>1E 1048.1-5937</i>							
No halo	1.55	1.06	1.5	0.7	9.5
Uniform	1.44	1.02	0.4	0.4	6.2	...	1.2
A	1.40	1.01	0.7	0.5	5.6	9.1	1.7
B	1.42	1.01	0.6	0.5	5.7	10.0	1.4
<i>1RXS J170849.0-400910</i>							
No halo	2.00	1.31	2.8	1.5	16.2
Uniform	1.83	1.24	0.8	0.9	8.5	...	1.2
A	1.91	1.27	1.3	1.1	5.8	3.2	2.6
B	1.78	1.23	1.1	1.0	8.1	3.9	1.7
C	1.78	1.23	0.9	0.9	8.9	4.0	1.8

NOTE. — These fits are for a dust size distribution $n(a) \propto a^{-3.5}$ between $a_{\text{min}} = 0.005$ and $a_{\text{max}} = 0.25 \mu\text{m}$. We omitted formal uncertainties, since they are typically substantially smaller than the differences between different models. The fluxes f are those of the unscattered component; the background surface brightnesses b have units of $10^{-6} \text{s}^{-1} \text{arcsec}^{-2}$.

^a For the 4U 0142+61 models with a ‘2’ suffix, the solution is that of a second minimum. See Fig. 2.

^b The number of degrees of freedom is 34 for the fits without halo, and 33 for fits with a halo model (38 data points, 4 or 5 fit parameters).

we reproduce the ratio of ~ 1.1 found by Katayama et al. between the background rate in the 4–7.2 keV range and that in the 1.7–4 keV range. From our calibrator, we find that for the bands we use, the ratio between the background counts with those in the 4–7.2 keV band are ~ 0.4 and 0.2 (for 1.2–1.6 and 2.0–2.4 keV, respectively; the ratio for the lower energy band is more uncertain, consistent with the finding of Katayama et al. (2004), who found that the background rate below 1.7 keV was poorly correlated with the rate at higher energies). We also find that all observations have similar 4–7.2 keV background count rates, of $1.5\text{--}2.5 \times 10^{-6} \text{s}^{-1} \text{arcsec}^{-2}$. Thus, the expected background rates in the 1.2–1.6 and 2.0–2.4 bands are also similar, ~ 0.8 and $0.4 \times 10^{-6} \text{s}^{-1} \text{arcsec}^{-2}$. This is roughly consistent both to what we listed above for the blank fields, and with what we infer from those of our fits that had acceptable χ^2 .

Overall, we conclude that the fact that we cannot measure the background rate directly, and thus have to leave it as a free parameter in our fits, affects the precision of our analysis, but has not introduced any major systematic uncertainties.

4.5. Model Caveats & Uncertainties

Our approach to fitting the halos has a number of potential pitfalls. First, our observations cover only part of the scattering halo: within the $\sim 3'$ covered by the data, only about 60% of the halo signal is contained (for uniformly distributed dust). However, to first order, this should just lead to large uncertainties, not large systematic errors: since we leave the background free, our limited coverage simply means it is easier to obtain an adequate fit. Furthermore, for our higher energy band, a bit

more of the halo is captured (about 75% for uniformly distributed dust).

Second, the model we used to fit the observed scattering halo is rather simplified and thus it is worthwhile to see what the possible systematic errors could be. One relatively small simplification is that we take the mean energy of all our photons to be that of the middle of a given energy band (and also use this to scale to the scattering optical depth from that at 1 keV). The associated error is likely small, however, since the count spectra of our sources show that the photon energy distribution is quite uniform over our 0.4 keV bands. (Note that we do integrate over the band for calculating the scattering halo, so include the small amount of “smearing” because of the change of energy.)

Another approximation we make is that we ignore multiple scattering. Mathis & Lee (1991) have shown that this dominates for $\tau_{\text{scat}} > 1.3$ or $A_V > 17$ mag at 1 keV. For our lowest energy band, at 1.4 keV, the use of the single-scattering approximation thus requires $A_V \ll 33$ mag, which is reasonably well satisfied for our sources.

The largest simplifications we make are the assumption of spherical dust grains with a power-law size distribution, and the treatment of scattering in the RG approximation. For the dust distribution, our two trial assumptions give significantly different results. We tried leaving the power-law index and limits free in our fits, but did not reach a clear conclusion. Generally, though, we would expect any systematic errors should be in the same direction for all sources, (unless dust properties vary significantly for different lines of sight, e.g., because one crosses a molecular cloud while another does not). Thus,

e.g., our conclusion that the total dust column towards 1E 1048.1–5937 is about 50% larger than that towards 4U 0142+61 should be reasonably safe. Indeed, as already mentioned in §2, since we use the calibration of the halo intensity with extinction of Predehl & Schmitt (1995), systematic errors may well be minimized by using simplifications as similar to theirs as possible, as we do.

Despite the above, ideally one would use physical models for the dust, such as that proposed by Weingartner & Draine (2001). Unfortunately, at present, our current understanding of dust scattering appears to be inadequate. For instance, Smith (2008) found that no model could reproduce in detail the dust scattering halo around GX 13+1, which he carefully measured in annuli ranging from 2 to 1000 arcsec. Smith also found that uniform dust distributions with power-law grain size distributions fitted the data as well as the presumably more physical models. Thus, at present, it seems one will have to continue to rely on empirical calibrations between halo intensity and optical depth or reddening.

5. CONCLUSIONS

We used *XMM* observations to measure the strengths of the scattering halos for three Anomalous X-ray Pulsars. In all three cases, we find that they are consistent with what was expected given extinctions determined previously from fits to the X-ray spectra. Combined with the run of extinction with distance, we thus also confirm the distances found by DvK06a. In particular, our results confirm that 1E 1048.1–5937 is much further than inferred by Gaensler et al. (2005) from a possible associ-

ation with an H I bubble.

Somewhat surprising is that the observed radial profiles are consistently fit as well or better by uniform dust distributions than they are by dust distributions that try to follow the actual run of extinction with distance inferred from red-clump stars. Part of the reason for the poorer fits for the presumably more realistic dust distributions may be that in our analysis we ignored complexities in the dust properties or the scattering process that might tend to smooth the radial profile, mimicking what would result from a more uniform dust distribution along the line of sight.

Nevertheless, our results suggest that, if one calibrates one's analysis method with a source with known extinction (4U 0142+61 in our case), it is possible to infer estimates of extinction columns to other sources good to about 20% from their scattering halos. With proper calibration, it should thus be possible to use the halos as independent constraints on model fits to the X-ray spectrum, and to help determine distances by comparing with the run of extinction with distance.

We thank Martin Durant and Peter Martin for discussions, the anonymous referee for a critical and constructive reading, as well as the *XMM* help desk for answering a number of queries. This work is based on observations obtained with *XMM-Newton*, an ESA science mission with instruments and contributions directly funded by ESA Member States and the USA (NASA).

Facilities: XMM (EPIC)

REFERENCES

- Carter, J. A. & Read, A. M. 2007, *A&A*, 464, 1155
 Costantini, E., Freyberg, M. J., & Predehl, P. 2005, *A&A*, 444, 187
 Durant, M. & van Kerkwijk, M. H. 2006a, *ApJ*, 650, 1070
 —. 2006b, *ApJ*, 650, 1082
 Gaensler, B. M., McClure-Griffiths, N. M., Oey, M. S., Haverkorn, M., Dickey, J. M., & Green, A. J. 2005, *ApJ*, 620, L95
 Ghizzardi, S. 2002, In flight calibration of the PSF for the PN camera, Calibration document XMM-SOC-CAL-TN-0029, European Space Agency
 Gregory, P. C. & Fahlman, G. G. 1980, *Nature*, 287, 805
 Henke, B. L., Lee, P., Tanaka, T. J., Shimabukuro, R. L., & Fujikawa, B. K. 1982, *Atomic Data and Nuclear Data Tables*, 27, 1
 Katayama, H., Takahashi, I., Ikebe, Y., Matsushita, K., & Freyberg, M. J. 2004, *A&A*, 414, 767
 Kothes, R., Uyaniker, B., & Yar, A. 2002, *ApJ*, 576, 169
 Mathis, J. S. & Lee, C.-W. 1991, *ApJ*, 376, 490
 Mathis, J. S., Rumpl, W., & Nordsieck, K. H. 1977, *ApJ*, 217, 425
 Mauche, C. W. & Gorenstein, P. 1986, *ApJ*, 302, 371
 Overbeck, J. W. 1965, *ApJ*, 141, 864
 Predehl, P., Burwitz, V., Paerels, F., & Trümper, J. 2000, *A&A*, 357, L25
 Predehl, P. & Schmitt, J. H. M. M. 1995, *A&A*, 293, 889
 Smith, R. K. 2008, *ApJ*, 681, 343
 Smith, R. K. & Dwek, E. 1998, *ApJ*, 503, 831
 Strüder, L. et al. 2001, *A&A*, 365, L18
 van de Hulst, H. C. 1957, *Light Scattering by Small Particles* (New York: John Wiley and Sons)
 Vasisht, G. & Gotthelf, E. V. 1997, *ApJ*, 486, L129+
 Weingartner, J. C. & Draine, B. T. 2001, *ApJ*, 548, 296
 Woods, P. M. & Thompson, C. 2006, in *Compact stellar X-ray sources*, ed. W. H. G. Lewin & M. van der Klis, 547–586
 Xiang, J., Lee, J. C., & Nowak, M. A. 2007, *ApJ*, 660, 1309